frontiers | Frontiers in Physics

TYPE Original Research
PUBLISHED 09 November 2023
DOI 10.3389/fphy.2023.1301453

OPEN ACCESS

EDITED BY
Felix Sharipov,
Federal University of Paraná, Brazil

REVIEWED BY
B. Venkateswarlu,
Yeungnam University, Republic of Korea
Andaç Batur Çolak,
Istanbul Commerce University, Türkiye
Wasfi Shatanawi,
Hashemite University, Jordan

*CORRESPONDENCE
Mahvish Samar,
mahvishsamar@hotmail.com

RECEIVED 25 September 2023
ACCEPTED 17 October 2023
PUBLISHED 09 November 2023

CITATION
Zulqarnain RM, Nadeem M, Siddique I, Samar M, Khan I and Mohamed A (2023), Numerical study of second-grade fuzzy hybrid nanofluid flow over the exponentially permeable stretching/shrinking surface.
Front. Phys. 11:1301453.
doi: 10.3389/fphy.2023.1301453

Numerical study of second-grade fuzzy hybrid nanofluid flow over the exponentially permeable stretching/shrinking surface

Rana Muhammad Zulqarnain[1], Muhammad Nadeem[2], Imran Siddique[2], Mahvish Samar[3]*, Ilyas Khan[4] and Abdullah Mohamed[5]

[1]School of Mathematical Sciences, Zhejiang Normal University, Jinhua, Zhejiang, China, [2]Department of Mathematics, University of Management and Technology, Lahore, Pakistan, [3]School of Computer Science and Technology, Zhejiang Normal University, Jinhua, Zhejiang, China, [4]Department of Mathematics, College of Science Al-Zulfi, Majmaah University, Al-Majmaah, Saudi Arabia, [5]Research Centre, Future University in Egypt, New Cairo, Egypt

The study of hybrid nanoliquids can aid in developing numerous advanced features that facilitate heat transmission, such as pharmaceutical processes, hybrid-powered engines, microelectronics, engine cooling, and domestic refrigerators. In the current study, a mathematical model is designed to elaborate the physical inception of an unsteady second-grade hybrid nanofluid with $Al_2O_3 - Cu/SA$, a combination concentrated over the permeable exponentially heated stretching/shrinking sheet under hydromagnetic, heat source/sink, and viscous dissipation implications. The set of similarity transforms is used to convert underlying partial differential equations into the system of ordinary differential equations. The well-known homotopy analysis method is applied to tackle the formulated differential system in the MATHEMATICA program, which can obtain non-uniqueness outcomes. The imprecision of nanofluid and hybrid nanofluid volume fractions was modeled as a triangular fuzzy number [0%, 5%, 10%] for comparison. The double parametric approach was applied to deal with the fuzziness of the associated fuzzy parameters. The nonlinear ordinary differential equations are converted into fuzzy differential equations, and the homotopy analysis method is used for the fuzzy solution. In terms of code validity, our results are matched to previous findings. The features of several parameters against the velocity, surface-friction coefficient, heat transfer, and Nusselt number are described via graphs. Furthermore, the nanoparticle volume fraction magnifies the fluid temperature and retards the flow profile throughout the domain, according to our findings. Thermal profiles increase with progress in the heat source, nanoparticles volumetric fractions, viscous dissipation, and nonlinear thermal radiation. The percentage increase in the drag force and heat transfer rate are 15.18 and 5.54 when the magnetic parameter takes input in the range $0.1 \leq M \leq 0.3$ and nanoparticle volume fraction inputs $0.01 \leq \phi_1 \leq 0.15$. From our observation, the

hybrid nanofluid displays the maximum heat transfer compared to nanofluids. This important contribution will support industrial growth, particularly in the processing and manufacturing sectors.

KEYWORDS

second-grade fluid, exponential stretching surface, thermal radiation, hybrid nanofluid, triangular fuzzy number (TFN)

1 Introduction

Investigations into non-Newtonian materials have been ongoing since the past century due to their unique characteristics and fascinating rheological properties. These materials are widely used across various industries, including chemical engineering, metal processing, food, and plastics. Non-Newtonian fluids have a range of applications, including biofluids, glassblowing, synthetic fibers, cosmetics, food, pharmaceuticals, shampoo, and metal spinning. These fluids exhibit different behaviors and can be classified as dilatant, shear-thickening, thixotropic, or shear-thinning. Rheologists have identified various fluid models, such as Casson, Maxwell, Burgers, Williamson, Oldroyd-B, third-grade, Jeffrey, micropolar, Sisko, and Sutterby Cross. However, second-grade fluids behave differently under different conditions, which explains the characteristics of shear-thickening, shear-thinning, and Newtonian effects. Second-grade fluids have gained the attention and devotion of intellectuals due to their dynamic properties [1–8]. Stretching a plastic sheet, on the other hand, is not always linear. An exponentially stretched sheet's heat transport characteristics have a broader range of technical applicability. The heat transfer ratio of the continuously expanded surface increases rapidly with the expansion rate and temperature variations, which regulates the outcome when the copper wire is thinned and diluted. The techniques involved in these methods significantly impact the final product quality due to the effect of stretching kinematics and concurrent heating or cooling. Khan and Sanjayanand [9] analyzed a second-grade fluid's steady flow and heat conductivity with an exponentially extending surface using the Runge–Kutta fourth-order (RK4) method. Rehman et al. [10] investigated the steady flow of a second-grade fluid over an exponentially stretching sheet using the Keller box and homotopy analysis approaches. Nadeem et al. [11] explored the flow and heat transfer of second-grade (viscoelastic) liquids in thermal radiation. Ramzan and Bilal [12] calculated the mixed convection of a second-grade nanofluid caused by time-dependent MHD, thermal radiation, and diffuse surfaces. Pakdemirli et al. [13] used perturbation analysis to examine the properties of a second-grade fluid. Recently, many researchers have studied second-grade nanofluids over an exponentially stretching surface [14–23].

Professionals like unsteady flow in several engineering organizations since it contributes to better mechanisms over their deeds [24, 25]. Moreover, even in ideal flow conditions, unnecessary destabilizing effects can occur around the system. The behavior of unstable boundary layer (BL) flow is unique compared to steady-state flow because the control equation has additional time-dependent conditions that degrade the structure of BL separation and fluid motion. However, through a healthier consideration of unstable fluid flow presentations in manufacturing dealings, contemporary enterprise techniques that permit improved structure dependability, productivity, and cost saving of multiple dynamical devices are possible [26]. Zaib et al. [27] discussed the computational exploration of a time-dependent flow with heat flux past an exponentially contracting surface.

The spectacle of heat transfer in electromagnetic waves is called thermal radiation. It happens because the two mediums have a significant temperature difference. In manufacturing and physical science, radiative influences are a crucial part. In the polymer manufacturing sectors, where heat-controlling variables influence the ultimate product quality to some extent, thermal radiation impacts are essential in controlling heat transfer. In addition, the radiation effects of missiles, aircraft, solar radiation, gas turbines, liquid metal fluids, spacecraft, nuclear power plants, and MHD accelerators are also prominent. Pantokratoras and Fang [28] were pioneers in examining the effect of nonlinear thermal radiation on Sakiadis flow. Dogonchi and Ganji [29] evaluated the impact of radiant heat on the MHD flow of a water-based nanofluid in a channel that can shrink, stretch, and diverge or converge. Khan et al. [30] studied the radiation flow of hybrid nanofluids through porous surfaces [30]. Many researchers [31–36] are involved in nonlinear thermal radiation.

Recognizing the need for improved thermal conductivity in traditional fluids, a new type of nanofluid called "hybrid nanofluid" is presented to provide highly industrialized heat conductivity. Two or more semiconductor materials are mixed with a base fluid to make a hybrid nanofluid. Different nanomaterials include carbon nanotubes [37], metals, metal oxides, and carbides. Numerous investigators are now interested in hybrid nanofluid due to its significance for the betterment of thermodynamic characteristics in real-world applications [38, 39], as a result of Choi and Eastman's [40] outstanding findings that gave the unique notion of nanoliquid. Hybrid nanofluids are also used in various applications, including electrical gadget cooling [41], cooling of domestic refrigerators [42], automobile braking fluid, transformers, heat exchangers, and solar water heating [43]. Suresh et al. [44] explored the effects of a hybrid nanofluid (Al_2O_3 + Cu/Water) in a circular tube that was uniformly heated. Momin [45] investigated the thermal act of a hybrid nanofluid in a spherical tube and demonstrated that the hybrid nanofluid improves thermal conductivity compared to a conventional working liquid. Waini et al. [46] explored the influence of buoyancy on hybrid (Al_2O_3 + Cu/Water) nanofluid flow toward the stagnation point of an exponentially stretching/shrinking vertical sheet. They determined that the (Al_2O_3 + Cu/Water) hybrid nanofluid had a greater rate of heat transfer than the Cu/water nanofluid. Khan [47] numerically examined the convection of copper (Cu + Water) and nanoliquid

across a spinning disc in a porous media. Cu–water has a faster heat transfer rate than Al_2O_3/Water, and the presence of porous media raised the thickness of the thermal boundary layer. Takabi and Salehi [48] analyzed the heat transfers of (Al_2O_3/Water) nanofluids and (Al_2O_3 + Cu/Water) hybrid nanofluids with a heat source. The literature is well stocked with further information on this topic [49–53].

The fuzzy set theory (FST) [54] has proved to be a valuable technique for modeling uncertainties in recent decades, providing models with a more accurate view of reality and allowing them to express themselves with a broader perspective [55–59]. After modeling real-world problems, they convert into partial differential equations (PDEs) or ordinary differential equations (ODEs). Uncertainty issues may arise during the development of a dynamic model. Researchers must deal with inaccurate data, parameters, dynamical variability, and complex relationships. As a result, many scientists use fuzzy models to depict dynamical systems to prevent artificial data accuracy and produce more realistic results. The fuzzy differential equation (FDE) is critical in overcoming these challenges. Initially, Chang and Zadeh [60] proposed the basic idea of fuzzy derivatives. Dubois and Prade [61] proposed the idea of fuzzy numbers (FNs) for solving an FDE. Kaleva [62] introduced the concept of FDEs in a fuzzy environment. Recently, FDEs played a significant role in fluid dynamics, such as the effects of MHD and gravitation on the third-grade fluid through an inclined channel in a fuzzy atmosphere, which were quantitatively explored by Nadeem et al. [63]. They used the triangular fuzzy numbers to analyze ambiguity. The heat transmission of SWCNTs MWCNTS on a third-grade nanofluid along an inclined channel in a fuzzy atmosphere was explored by Siddiqui et al. [64]. For comparison and uncertainty, they used nanoparticle volume fraction as TFN.

A careful review of the previously cited literature reveals several breaks and confines. No preceding studies have examined the unsteady MHD flow of the second-grade hybrid (Al_2O_3 – Cu/SA) nanofluid over the exponentially stretching/shrinking sheet with heat source/sink and viscous dissipation in their research outline. Also, the nanoparticle volume fraction of nanofluid and hybrid nanofluid are taken as triangular fuzzy numbers using the double parametric concept for comparison and uncertainty. The homotopy analysis technique was used to tackle the problem under consideration. The impact of important parameters on heat and flow field quantities and nanoparticle volume fraction is graphed and briefly discussed. This innovative contribution might help improve industrial manufacturing, predominantly in the processing and industrial areas.

The motivations for performing this analysis inspire the following research questions:

1) How do the thermal characteristics of nanoparticles vary when nonlinear thermal radiation features are used?
2) How do different developing parameters affect heat transfer and flow rates?
3) How does heat transfer improve in heat source/sink and magnetic force implications?
4) Why is the homotopy analysis method (HAM) preferred over the other methods?
5) Ho\w does the Lorentz force affect the velocity of the second-grade hybrid nanofluid by applying the magnetic field?

2 Mathematical formulation

The time-dependent, 2D incompressible, and unsteady flow of the MHD viscoelastic (second-grade) hybrid Al_2O_3 + Cu/SA nanofluid over the exponentially stretching/shrinking surface is engaged into interpretation in this research, as shown in Figure 1. $u_w(x,t) = \lambda e^{x/L}(a/(1-ct))$ signifies the stretching/shrinking velocity, where lambda represents a constant that relates to stretching $\lambda > 0$. In shrinking $\lambda < 0$ cases of the velocity rate, L indicates the characteristic length and c denotes the unsteadiness. $v_w(x,t) = (v_o e^{x/2L}/\sqrt{1-ct})$ signifies the mass flux velocity, where v_o is the constant. The ambient and reference temperatures are labeled as T_w and T_∞, correspondingly, while $T_w = T_\infty + e^{x/2L}(T_o/(1-ct))$ regulates the temperature circulation close to the surface. The magnetic field is expected to be $B(x) = e^{x/2L}(B_o/\sqrt{(1-ct)})$, with B_o indicating an identical magnetic field. The viscous, source/sink, and nonlinear thermal radiation impacts are also deliberated.

When using the BL approximation, the governing equations for continuity, momentum, and heat are established on all of the preceding assumptions [12, 51]:

$$\frac{\partial v}{\partial y} + \frac{\partial u}{\partial x} = 0, \tag{1}$$

$$\frac{\partial u}{\partial t} + u\frac{\partial u}{\partial x} + v\frac{\partial u}{\partial y} = \frac{\mu_{hnf}}{\rho_{hnf}}\frac{\partial^2 u}{\partial y^2} + \frac{\alpha_1}{\rho_{hnf}}\left(\frac{\partial^3 u}{\partial t \partial y^3} + u\frac{\partial^3 u}{\partial x \partial y^3} + \frac{\partial u}{\partial x}\frac{\partial^2 u}{\partial y^2} + \frac{\partial u}{\partial y}\frac{\partial^2 v}{\partial y^2} + v\frac{\partial^3 u}{\partial y^3}\right) - \frac{\sigma_{hnf}}{\rho_{hnf}}B_0^2 u, \tag{2}$$

$$u\frac{\partial T}{\partial x} + v\frac{\partial T}{\partial y} + \frac{\partial T}{\partial t} = \alpha_{hnf}\frac{\partial^2 T}{\partial y^2} + \frac{Q_0(T-T_\infty)}{(\rho c_P)_{hnf}} + \frac{16\delta^*}{3k^*(\rho c_P)_f}\left(T^3\frac{\partial^2 T}{\partial y^2} + 3T^2\left(\frac{\partial T}{\partial y}\right)^2\right) + \frac{\mu_{hnf}}{(\rho c_P)_{hnf}}\left(\frac{\partial u}{\partial y}\right)^2 + \frac{\alpha_1}{(\rho c_P)_{hnf}}\left(\frac{\partial u}{\partial y}\frac{\partial^2 u}{\partial y \partial t} + u\frac{\partial u}{\partial y}\frac{\partial^2 u}{\partial x \partial y} + v\frac{\partial u}{\partial y}\frac{\partial^2 u}{\partial y^2}\right), \tag{3}$$

and the boundary conditions are

$$\left.\begin{array}{l} t<0:\ T = T_\infty,\ v = 0, u = 0,\ \forall x, y, \\ t \geq 0:\ v = v_w,\ u = U_w(x,t) = \lambda u_w(x,t),\ T = T_w \quad \text{at } y \to 0, \\ u = 0,\ T = T_\infty \quad \text{as} \quad y \to \infty, \end{array}\right\} \tag{4}$$

where u and v indicate the velocity components along the $x-$ axis and $y-$ axis, respectively, while the fluid temperature is denoted by T. The dynamic viscosity Al_2O_3 + Cu/SA is μ_{hnf}, ρ_{hnf} is the density of Al_2O_3 + Cu/SA, $(\rho Cp)_{hnf}$ is the Al_2O_3 + Cu/SA heat capacity, k_{hnf} is the Al_2O_3 + Cu/SA thermal/heat conductivity, and δ_{hnf} is the electrical conductivity Al_2O_3 + Cu/SA. The aluminum oxide (Al_2O_3) thermophysical properties, along with copper (Cu) and sodium alginate (SA) nanoparticles, are revealed in Table 1. Equation (5) contains the thermophysical properties of Al_2O_3 + Cu/SA. Here, Al_2O_3 and Cu are nanoparticles having the volume fractions ϕ_1 and ϕ_2, respectively.

The thermophysical properties of hybrid nanofluids are as follows [51]:

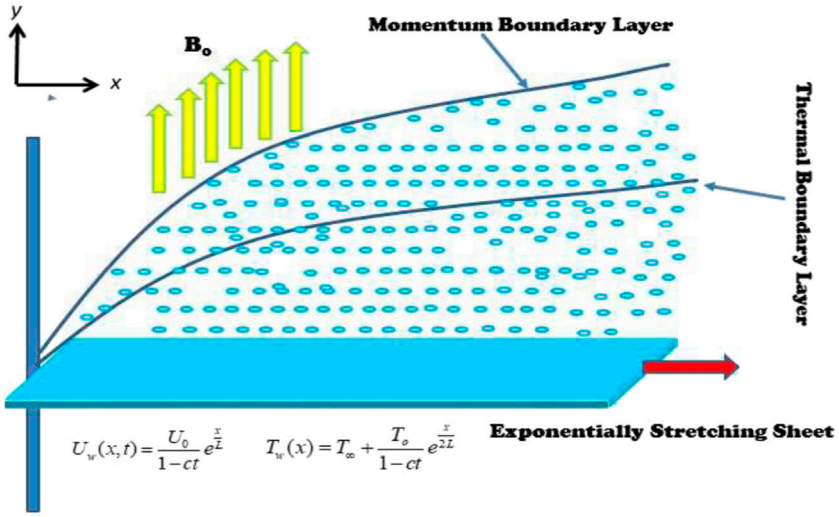

FIGURE 1
Flow problem.

TABLE 1 Al_2O_3 thermophysical properties along with *Cu* and SA [51].

Physical properties	$\rho\,(kg/m^3)$	$\rho c_p\,(J/kgK)$	$k\,(W/mK)$	$\beta_T \times 10^{-5}\,(1/K)$	$\sigma\,(\Omega/m)^{-1}$
SA	989	4,175	0.6376	99	2.6×10^{-4}
Al_2O_3	3,970	765	40	0.85	3.69×10^{7}
Cu	8,933	385	401	1.67	5.96×10^{7}

$$\left.\begin{aligned}
&\rho_r=\frac{\rho_{hnf}}{\rho_f}=\left[(1-\phi_2)\left\{(1-\phi_1)+\frac{\rho_{s_1}\phi_1}{\rho_f}\right\}+\frac{\rho_{s_2}\phi_2}{\rho_f}\right],\mu_r=\frac{\mu_{hnf}}{\mu_f}=(1-\phi_1)^{-2.5}(1-\phi_2)^{-2.5},\\
&\left(\rho C_\rho\right)_r=\frac{\left(\rho C_\rho\right)_{hnf}}{\left(\rho C_\rho\right)_f}=\frac{\phi_2\left(\rho C_\rho\right)_{s_2}}{\left(\rho C_\rho\right)_f}+(1-\phi_2)\left[(1-\phi_1)+\frac{\left(\rho C_\rho\right)_{s_1}\phi_1}{\left(\rho C_\rho\right)_f}\right],\\
&k_r=\frac{k_{hnf}}{k_{nf}}=\frac{2k_{nf}-2\phi_1\left(k_{s_1}-k_{nf}\right)+k_{s_1}}{2k_{nf}+\phi_1\left(k_{s_1}-k_{nf}\right)+k_{s_1}},\frac{k_{nf}}{k_f}=\frac{2k_f-2\phi_2\left(k_{s_2}-k_f\right)+k_{s_2}}{2k_f+\phi_2\left(k_{s_2}-k_f\right)+k_{s_2}},\\
&\sigma_r=\frac{\sigma_{hnf}}{\sigma_{bf}}=\left[\frac{\sigma_{s_2}(1+2\phi_2)+2\sigma_{bf}(1-\phi_2)}{\sigma_{s_2}(1-\phi_2)+\sigma_{bf}(2+\phi_2)}\right],\sigma_{bf}=\left[\frac{\sigma_{s_1}(1+2\phi_1)+2\sigma_f(1-\phi_1)}{\sigma_{s_1}(1-\phi_1)+\sigma_f(2+\phi_1)}\right]\sigma_f.
\end{aligned}\right\} \tag{5}$$

The following similarity transformations are presented in [10] to simplify the governing Eqs 1–3 along with the boundary conditions (4). The stream function ω can be expressed as a customizable form $v=-\partial\omega/\partial x, u=\partial\omega/\partial y$, and the similarity variable is η:

$$\left.\begin{aligned}
&\omega=\sqrt{\frac{2la\nu_f}{1-ct}}e^{x/2L}f(\eta),\eta=\sqrt{\frac{a}{2l\nu_f(1-ct)}}e^{x/2L}y,\theta(\eta)=\frac{T-T_\infty}{T_w-T_\infty},\\
&u=\frac{ae^{\frac{x}{L}}}{1-ct}f'(\eta),v=-\sqrt{\frac{a\nu_f}{2l(1-ct)}}e^{x/2L}\left(f(\eta)+\eta f'(\eta)\right).
\end{aligned}\right\} \tag{6}$$

Using Eq. 6, Eqs (2), (3) can be condensed to the following set of nonlinear ODEs in the context of the abovementioned relations [36]:

$$\left(\frac{\mu_r}{\rho_r}\right)f'''-2(f')^2-\beta\left(\frac{\eta}{2}f''+f'\right)+ff''+\frac{\alpha}{\rho_r}\left(\beta f'''+2f'f'''-(f'')^2-ff^{iv}+\frac{\beta\eta}{2}f^{iv}\right)-\frac{\sigma_r}{\rho_r}Mf'=0, \tag{7}$$

$$(1+\mathrm{Nr}(1+\theta(\theta_w-1))^3)\theta''+3\mathrm{Nr}(\theta')^2(\theta_w-1)(1+\theta(\theta_w-1))^2+\mathrm{Pr}f\theta'-\mathrm{Pr}\beta\left(\frac{1}{2}\eta\theta'+\theta\right)-\mathrm{Pr}\theta f'+\frac{\mathrm{PrH}\theta}{(\rho c_P)_r}+\frac{\mu_r\mathrm{PrEc}}{(\rho c_P)_r}(f'')^2+\frac{\alpha\mathrm{PrEc}}{(\rho c_P)_r}f''(2\eta f''+2f'f''-ff'''+\eta\beta f''')=0, \tag{8}$$

with the constraints

$$\left.\begin{aligned}
&f(\eta)=s,\ f'(\eta)=\lambda,\theta(\eta)=1 \quad \text{at} \quad \eta=0,\\
&f'(\eta)=0,\ \theta(\eta)=0 \quad\quad\quad \text{as} \quad \eta\to\infty.
\end{aligned}\right\}, \tag{9}$$

where the unsteadiness parameter is $\beta=2Lc/ae^{\frac{x}{L}}$, the magnetic parameter is $M=2\delta_f LB_o^2/a\rho_f$, the Prandtl number is $\mathrm{Pr}=\nu_f/\alpha_f$, the second-grade fluid parameter is $\alpha=ae^{x/L}/2L\mu_f(1-ct)$, the Eckert number is $Ec=a^2/(1-\mathrm{ct})^2(T_w-T_\infty)(C_\rho)_f$, the heat generation/absorption parameter is $H=2L(1-\mathrm{ct})(T_w-T_\infty)Q_o/a$, and the suction parameter is $s=-v_o\sqrt{2L/a\nu_f}$.

The stretching/shrinking parameter is λ. The coefficient of skin friction (C_{fx}) and the local Nusselt number (Nu_x) are, thus, demarcated as follows [12]:

$$C_{fx}=\frac{1}{\rho_f u_e^2}\left[\mu_{hnf}\frac{\partial u}{\partial y}+\alpha_1\left\{u\frac{\partial^2 u}{\partial x\partial y}+v\frac{\partial^2 u}{\partial y^2}+\frac{\partial^2 u}{\partial t\partial y}+2\frac{\partial u}{\partial y}\frac{\partial u}{\partial x}\right\}\right]_{y=0}, \tag{10}$$

$$Nu_x=-\frac{x}{k_f(T_w-T_\infty)}\left[k_{hnf}\frac{\partial T}{\partial y}+\frac{16\sigma^\star T_\infty^3}{3k^\star}\frac{\partial T}{\partial y}\right]_{y=0}. \tag{11}$$

Using Eq. 6 in Eq. 10 and Eq. (11) yields the following relationship:

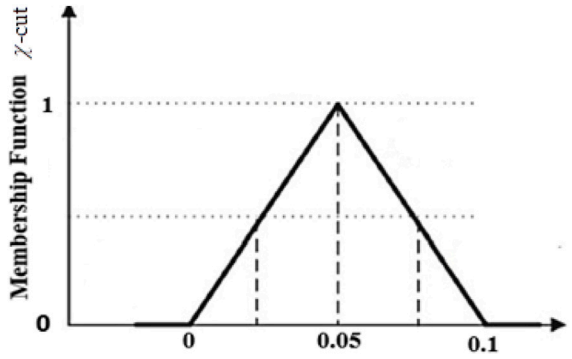

FIGURE 2
Membership function of TFN [54].

$$\sqrt{\mathrm{Re}_x}C_{fx} = \left(\mu_r f''(0) + \alpha\left(7f'(0)f''(0) - f(0)f''(0) + 3\beta f''(0) + \eta f''(0)f''(0) + \eta\beta f'''(0)\right)\right), \tag{12}$$

$$(\mathrm{Re}_x)^{-0.5}Nu_x = -\left(k_r + Nr\left(1+\theta(0)(\theta_w-1)\right)^3\right)\theta'(0), \tag{13}$$

where $Re_x = u_e x/\nu_f$ is the x-axis-local Reynolds number. Moreover, the graphical explaination of triangular fuzzy number is given in the Figure 2.

2.1 Homotopy analysis method

The HAM is a multifaceted investigative system that solves nonlinear equations with several variables. Based on Eq. 9, the HAM computes consequential Eqs 7, 8. Linear operators and preliminary approximations are mandatory to surprise the process through this technique. Consequently, we used them as $(\Lambda_f, \Lambda_\theta)$ linear operators and $(f_0(\eta), \theta_0(\eta))$ initial assessments to resolve motion and energy transform equations using the abovementioned method. See [9–12] for further facts on this method.

$$f_0(\eta) = s - \lambda(1 - e^{-\eta}),\ \theta_0(\eta) = e^{-\eta}, \tag{14}$$

$$\Lambda_f[f(\eta)] = f''' - f',\ \Lambda_\theta[\theta(\eta)] = \theta'' - \theta. \tag{15}$$

The properties of the operator described above are as follows:

$$\left.\begin{aligned}\Lambda_f(A_1 + A_2e^{-\eta} + A_3e^{\eta}) = 0,\\ \Lambda_\theta(A_4e^{-\eta} + A_5e^{\eta}) = 0,\end{aligned}\right\} \tag{16}$$

where A_{js} (j = 1, 2, 5) are arbitrary constants.

$$\left.\begin{aligned}(1-q)\Lambda_f\left[\tilde{F}(\eta;q) - \tilde{f}_0(\eta)\right] - qh_f N_f\left[\tilde{F}(\eta;q)\right] = 0,\\ (1-q)\Lambda_\theta\left[\tilde{\theta}(\eta;q) - \tilde{\theta}_0(\eta)\right] - qh_\theta N_\theta\left[\tilde{F}(\eta;q), \tilde{\theta}(\eta;q)\right] = 0,\end{aligned}\right\} \tag{17}$$

where h_f and h_θ signify non-zero auxiliary parameters, $q \in [0,1]$ represents an embedding parameter, and $\tilde{F}$, and $\tilde{\theta}$ represent the mapping occupations for $f(\eta)$, and $\theta(\eta)$, respectively.

The boundary conditions become [12]

$$\left.\begin{aligned}\tilde{F}(0;q) = s, \tilde{F}'(0;q) = \lambda, \tilde{\theta}(0;q) = 1,\\ \tilde{F}'(\infty;q) = 0, \tilde{\theta}(\infty;q) = 0,\end{aligned}\right\} \tag{18}$$

$$N_f\left[\tilde{F}(\eta;q)\right] = \frac{d\tilde{F}'''(\eta;q)}{d\eta} - 2\left(\frac{d\tilde{F}'(\eta;q)}{d\eta}\right)^2 + \frac{d\tilde{F}(\eta;q)}{d\eta}\frac{d\tilde{F}''(\eta;q)}{d\eta} - \beta\left(\frac{d\tilde{F}'(\eta;q)}{d\eta} + \frac{\eta}{2}\frac{d\tilde{F}''(\eta;q)}{d\eta}\right) + \alpha\left(\beta\frac{d\tilde{F}'''(\eta;q)}{d\eta} - \left(\frac{d\tilde{F}''(\eta;q)}{d\eta}\right)^2 - \tilde{F}(\eta;q)\frac{d\tilde{F}''''(\eta;q)}{d\eta} + 2\frac{d\tilde{F}'(\eta;q)}{d\eta}\frac{d\tilde{F}'''(\eta;q)}{d\eta} + \frac{\beta\eta}{2}\frac{d\tilde{F}''''(\eta;q)}{d\eta}\right) - M\frac{d\tilde{F}'(\eta;q)}{d\eta}, \tag{19}$$

$$\begin{aligned}N_\theta\left[\tilde{F}(\eta;q),\tilde{\theta}(\eta;q)\right] = &\left(1+\mathrm{Nr}\left(1+\tilde{\theta}(\eta;q)(\theta_w-1)\right)^3\right)\frac{d\tilde{\theta}''(\eta;q)}{d\eta} - \mathrm{Pr}\tilde{\theta}(\eta;q)\frac{d\tilde{F}'(\eta;q)}{d\eta}\\ &+3\mathrm{Nr}\left(\frac{d\tilde{\theta}'(\eta;q)}{d\eta}\right)^2(\theta_w-1)\left(1+\tilde{\theta}(\eta;q)(\theta_w-1)\right)^2\\ &+\mathrm{Pr}D\tilde{F}(\eta;q)\frac{d\tilde{\phi}''(\eta;q)}{d\eta} + \mathrm{Pr}\tilde{F}(\eta;q)\frac{d\tilde{\theta}'(\eta;q)}{d\eta} + \mathrm{PrEc}\left(\frac{d\tilde{F}''(\eta;q)}{d\eta}\right)^2\\ &-\mathrm{Pr}\beta\left(\frac{1}{2}\eta\frac{d\tilde{\theta}'(\eta;q)}{d\eta} + \tilde{\theta}(\eta;q)\right) + \alpha\mathrm{PrEc}\frac{d\tilde{F}''(\eta;q)}{d\eta}\\ &\left(\begin{aligned}&2\eta\frac{d\tilde{F}''(\eta;q)}{d\eta} + 2\frac{d\tilde{F}'(\eta;q)}{d\eta}\frac{d\tilde{F}''(\eta;q)}{d\eta}\\ &+\eta\beta\frac{d\tilde{F}'''(\eta;q)}{d\eta} - \tilde{F}(\eta;q)\frac{d\tilde{F}'''(\eta;q)}{d\eta}\end{aligned}\right)\\ &+\mathrm{Pr}\frac{d\tilde{\theta}'(\eta;q)}{d\eta}\left(Nb\frac{d\tilde{\phi}'(\eta;q)}{d\eta} + Nt\frac{d\tilde{\theta}'(\eta;q)}{d\eta}\right).\end{aligned} \tag{20}$$

Equations (7)–(9) convert into nonlinear operators like Eqs 18–21, and then, the series solution becomes

$$\left.\begin{aligned}f(\eta) = f_0(\eta) + \sum_{m=1}^{\infty} f_m(\eta),\\ \theta(\eta) = \theta_0(\eta) + \sum_{m=1}^{\infty}\theta_m(\eta).\end{aligned}\right\} \tag{21}$$

2.2 Fuzzification

Using fuzzy concepts, comparing nanofluid and hybrid nanofluid is also explored in this study. The nonlinear ODEs convert into FDEs, and the nanoparticle volume percentage is taken as a TFN. The governing FDE is converted into a double parametric form. In this case, Eq. 8 can be converted into an interval form using the χ – cut concept. Here, χ and ω are parameters that range from 0 to 1, controlling the fuzziness of the uncertain parameters. The aforementioned problem was solved using the HAM as well. The slight variation in the volume percentage of nanoparticles impacts the flow rate and heat. These parameters alone determine the nanofluid's flow rate and heat transfer because some researchers estimate that the volume percentage of nanoparticles falls within the [1%–4%] range. It is preferable to address a challenging situation in a fuzzy atmosphere by getting volume fractions as a TFN since ϕ_1 and ϕ_2 signify the volume fraction of Al_2O_3/SA and Cu/SA, respectively, as shown in Table 2. The volume fractions of nanoparticles used in this study are classified as TFNs, with the TFNs being transformed into χ – cut methods, and the fuzziness of the TFNs is controlled by χ – cut [64].

TABLE 2 ϕ_1 **and** ϕ_2 **transform into TFN [54, 55].**

Fuzzy numbers	Crisp value	TFN	χ – cut approach
ϕ_1 (Al_2O_3)	[0.01–0.04]	[0, 0.05, 0.1]	$[0.05\chi, 0.1 - 0.05\chi], \chi \in [0,1]$
ϕ_2 (Cu)	[0.01–0.04]	[0, 0.05, 0.1]	$[0.05\chi, 0.1 - 0.05\chi], \chi \in [0,1]$

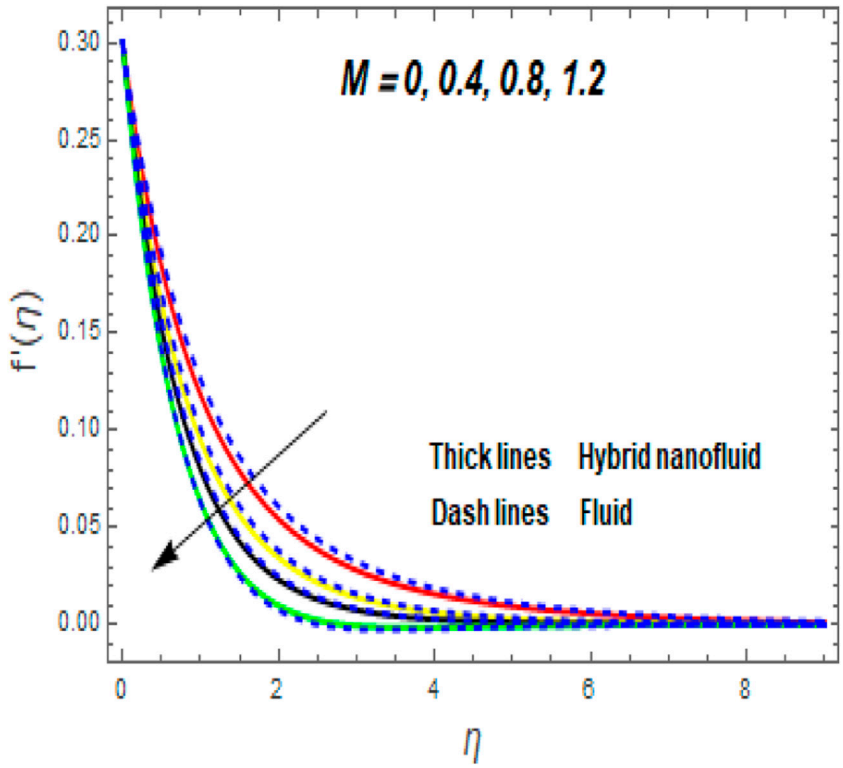

FIGURE 3
Impression of $f'(\eta)$ for M.

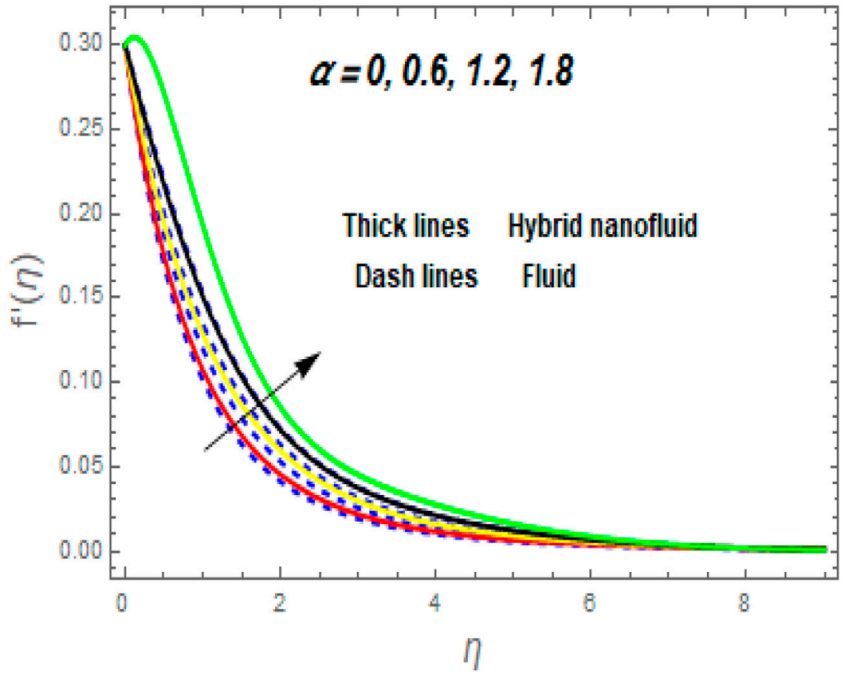

FIGURE 4
Impression of $f'(\eta)$ for α.

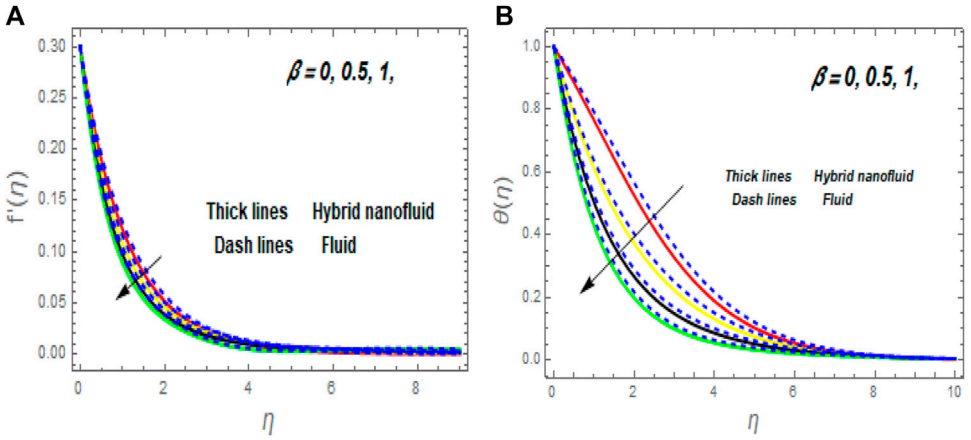

FIGURE 5
Impression of $f'(\eta)$ **(A)** and $\theta(\eta)$ **(B)** for β.

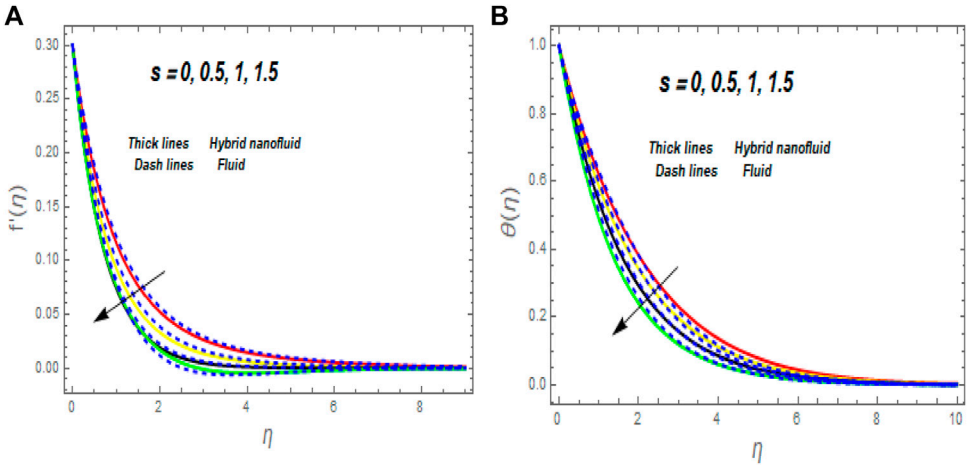

FIGURE 6
Impression of $f'(\eta)$ **(A)** and $\theta(\eta)$ **(B)** for s.

Let $\phi_1 = \phi_2 = [0, 0.05, 0.1]$ be a TFN that is described by the three values highlighted in Figure 3: 0 (lower bound), 0.05 (most belief value), and 0.1 (upper bound). As the input value moves from position 0 to position 0.05, the value of the membership function climbs linearly from 0 to 1 and then linearly declines from 1 to 0 as the input value moves from position 0.05 to position 0.1. Eq. 22 represents the mathematical form of the triangular fuzzy membership function as follows:

$$\text{Membership function} = \begin{cases} \dfrac{0-\eta}{0.05-0} & \text{for} \quad \eta \in [0, 0.05], \\ \dfrac{\eta-0.1}{0.1-0.05} & \text{for} \quad \eta \in [0.05, 0.1], \\ 0, \ \text{otherwise}. \end{cases} \tag{22}$$

The χ − cut technique is used to convert TFNs into an interval form and is represented as $\phi_1 = \phi_2 = [0 + \chi(0.05 - 0), 0.1 - \chi(0.1 - 0.05)]$, where $0 \leq \chi - \text{cut} \leq 1$.

To handle this scenario, the FDEs are renewed into lower $\theta_1(\eta, \chi)$ and upper $\theta_2(\eta, \chi)$ bounds.

3 Results and discussion

An unsteady flow analysis was performed on a second-grade hybrid (Al_2O_3 − Cu/SA) nanofluid above the exponential surface. Because of the viscous and nonlinear radiation heat transfer amalgamation, conductive fluids are studied in this context. The consequence of dynamic parameters on the speed and temperature profile of the system is scrutinized. In addition, an estimated analysis method called the HAM is used to follow the transformation equation generated from the abovementioned model. For the simulation of our model, we absolute the key parameters, such as $M = 0.2$, $\beta = 0.5$, $\alpha = 0.2$, $s = 0.2$, $Pr = 10$, $\theta_w = 1.2$, $Ec = 0.3$, $H = 0.1$, $\lambda = 0.3$, $\phi_1 = 0.02$, and $\phi_2 = 0.02$. Table 2 is created to confirm the values of $\theta'(0)$ [36]. The values obtained by the HAM in the current survey agree well with the literature.

The influence of the magnetic (M) parameter on the velocity field is depicted in Figure 3. For higher values of M, the velocity dropped in both cases. Lorentz pressure is responsible for this phenomenon, which arises

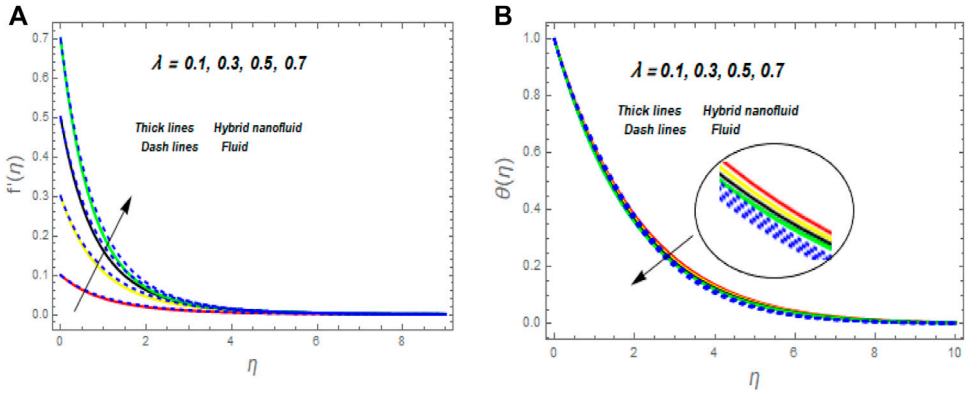

FIGURE 7
Impression of $f'(\eta)$ **(A)** and $\theta(\eta)$ **(B)** for λ.

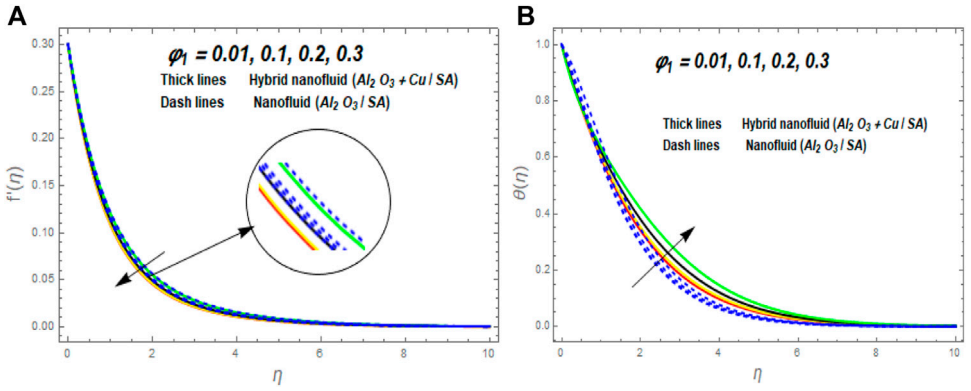

FIGURE 8
Impression of $f'(\eta)$ **(A)** and $\theta(\eta)$ **(B)** for ϕ_1.

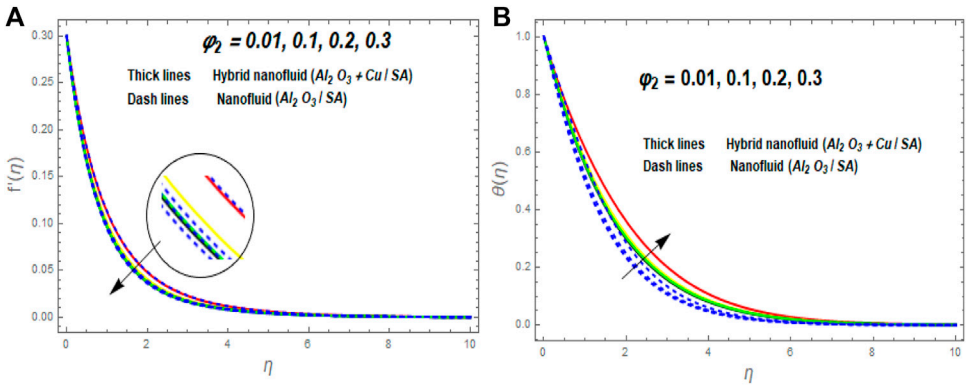

FIGURE 9
Impression of $f'(\eta)$ **(A)** and $\theta(\eta)$ **(B)** for ϕ_2.

from the cooperation of electric and magnetic fields during an electrically conducted fluid flow. So, the fluid velocity in the BL is controlled by the generated Lorentz force. As a result, as M rises, the velocity of the fluid and hybrid nanofluids falls. The interaction of magnetic fields is significant in different technical and industrial applications, such as crude oil extraction, geothermal systems, and groundwater hydrology.

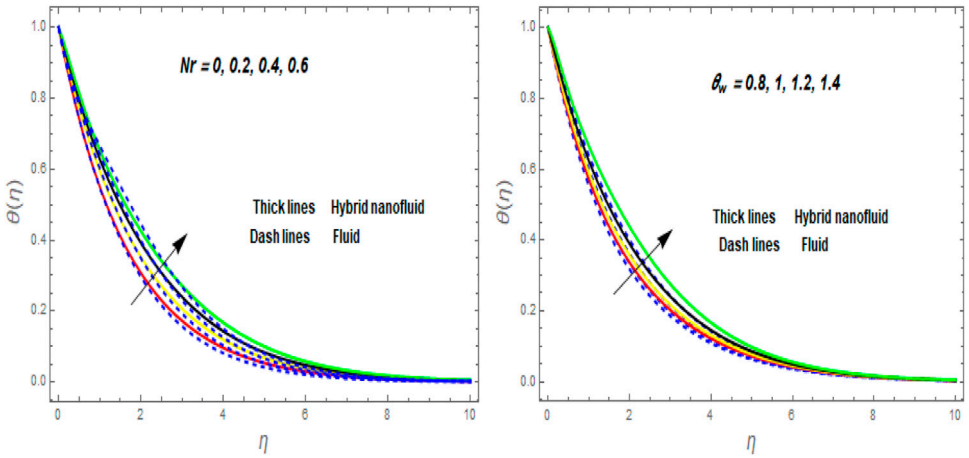

FIGURE 10
Impression of $\theta(\eta)$ for Nr and θ_w.

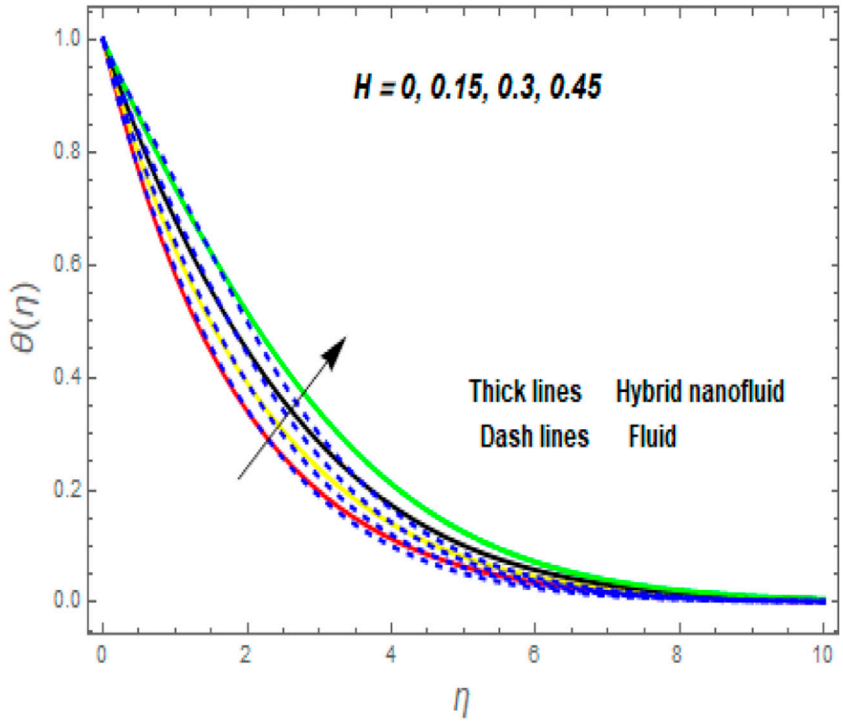

FIGURE 11
Impression of $\theta(\eta)$ for H.

The change of the second-grade parameter (α) in motion is shown in Figure 4. The rise in α clues to an enrichment in the velocity of liquid and hybrid nanofluids. This is because as α increases, the viscosity and viscous forces of the fluid decrease. The effects of an unsteady parameter (β) and suction parameter (s) on velocity and temperature fields are shown in Figures 5, 6. The temperature and velocity contours drop when β and s are increasing. The increase in β and s decreases the momentum and thermal boundry layer. Figure 7 shows the impression of stretching/shrinking parameters (λ) on velocity and temperature dispersals. When λ increases, the velocity also increases while the temperature diminishes. Because the stretching parameters are set to higher levels, the temperature and thickness of the BL are reduced. Due to the exposure of the cooler to the ambient fluid, the BL thickness reduces with growing values of stretching parameters. Figure 8 shows the variation of nanoparticle volume fraction (ϕ_1) on the velocity and temperature distributions. When ϕ_1 increases, the velocity declines while the temperature boosts up. The variability of the volume fractional of nanoparticles (ϕ_2) on velocity and temperature gradients is shown in

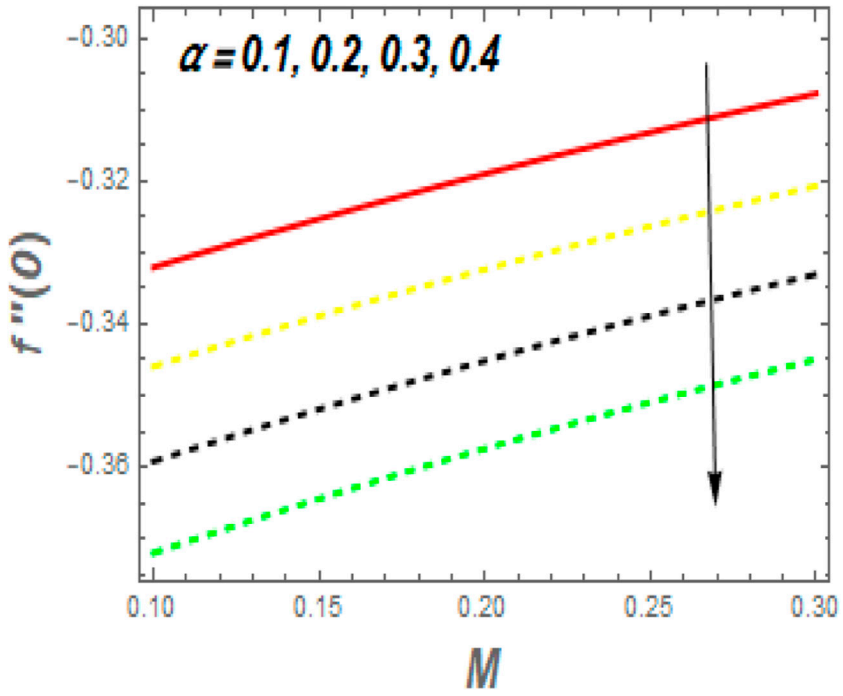

FIGURE 12
Impression of M and α on C_f.

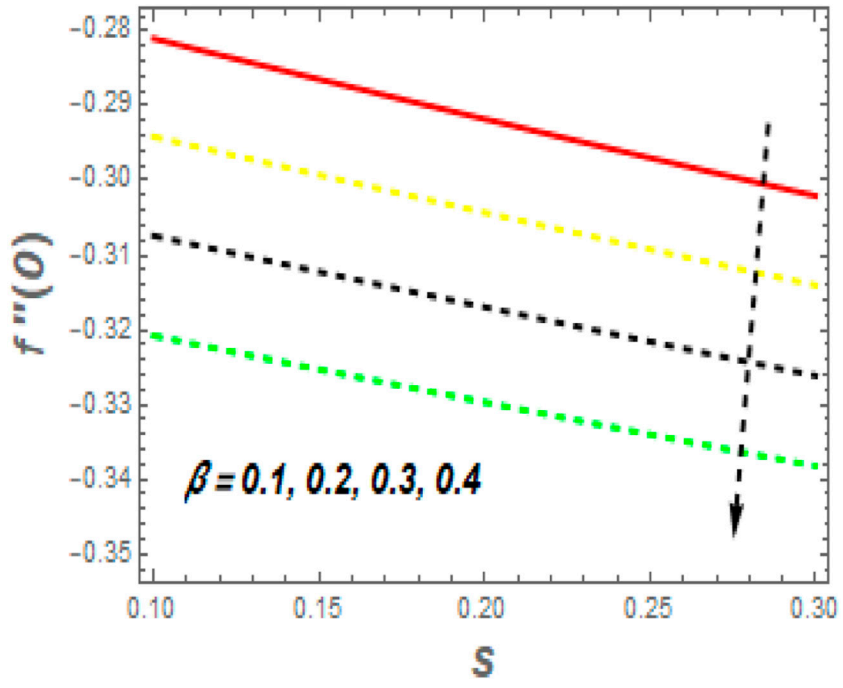

FIGURE 13
Impression of s and β on C_f.

Figure 9. When ϕ_2 progress, speed drops while temperature upsurges. The main reason for the decay in the velocity is that as the values of the volume fractional of nanoparticle grow, the resistive force also increases, reducing the fluid flow speed. Physically, the energy is discharged from the exponential sheet due to the nanoparticle's resistive force. More energy is generated when more nanoparticles are added, causing the temperature to rise. Furthermore, the optimum temperature may be achieved because a hybrid nanofluid has a higher thermal conductivity

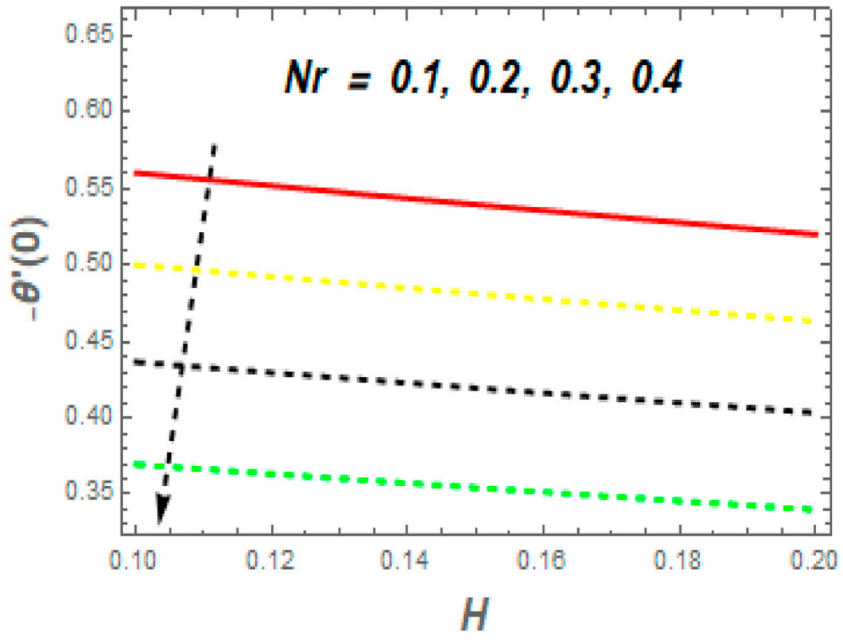

FIGURE 14
Impression of *Nr* and *H* on *Nu*.

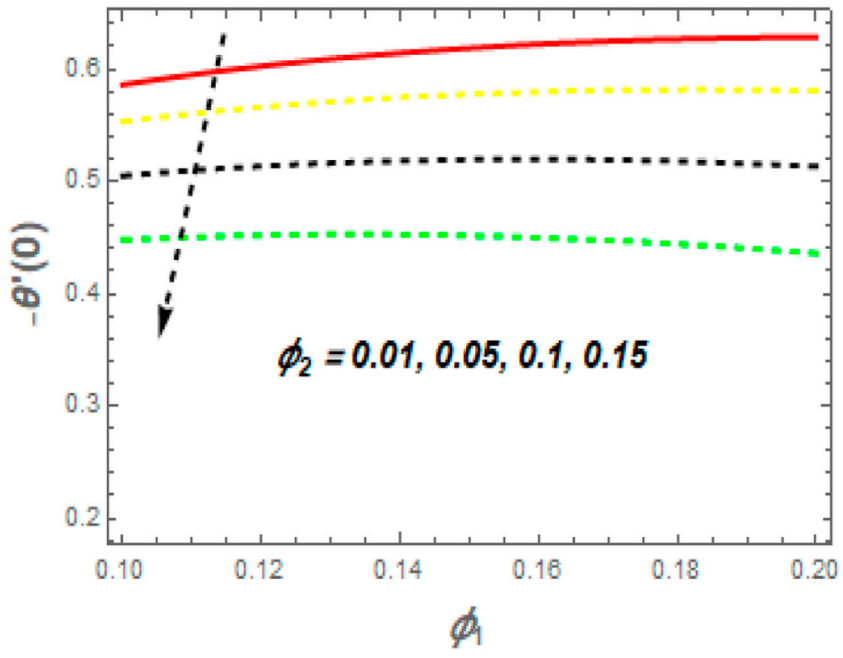

FIGURE 15
Impression of ϕ_1 and ϕ_2 on *Nu*.

than a mono nanofluid. Figure 10 shows the features of radiation parameters *(Nr)* and liquid temperature. High *Nr* approximations support the random motion of particles. As a result, more particles collide and produce more heat. As a result, the heat of the fluid increases. Figure 10 shows the thermal profile matures when the temperature ratio parameter (θ_w) rises. These consequences specified that when θw develops, the temperature difference $(T_w - T_0)$ upsurges, instigating the fluid temperature to increase. Figure 11 pierces the heat generation parameter (H) impressions on the temperature field. It is noticed that as the $H > 0$ grows, the temperature distribution improves. Physically, higher heat production shows more heat within the boundary layer, increasing the temperature field.

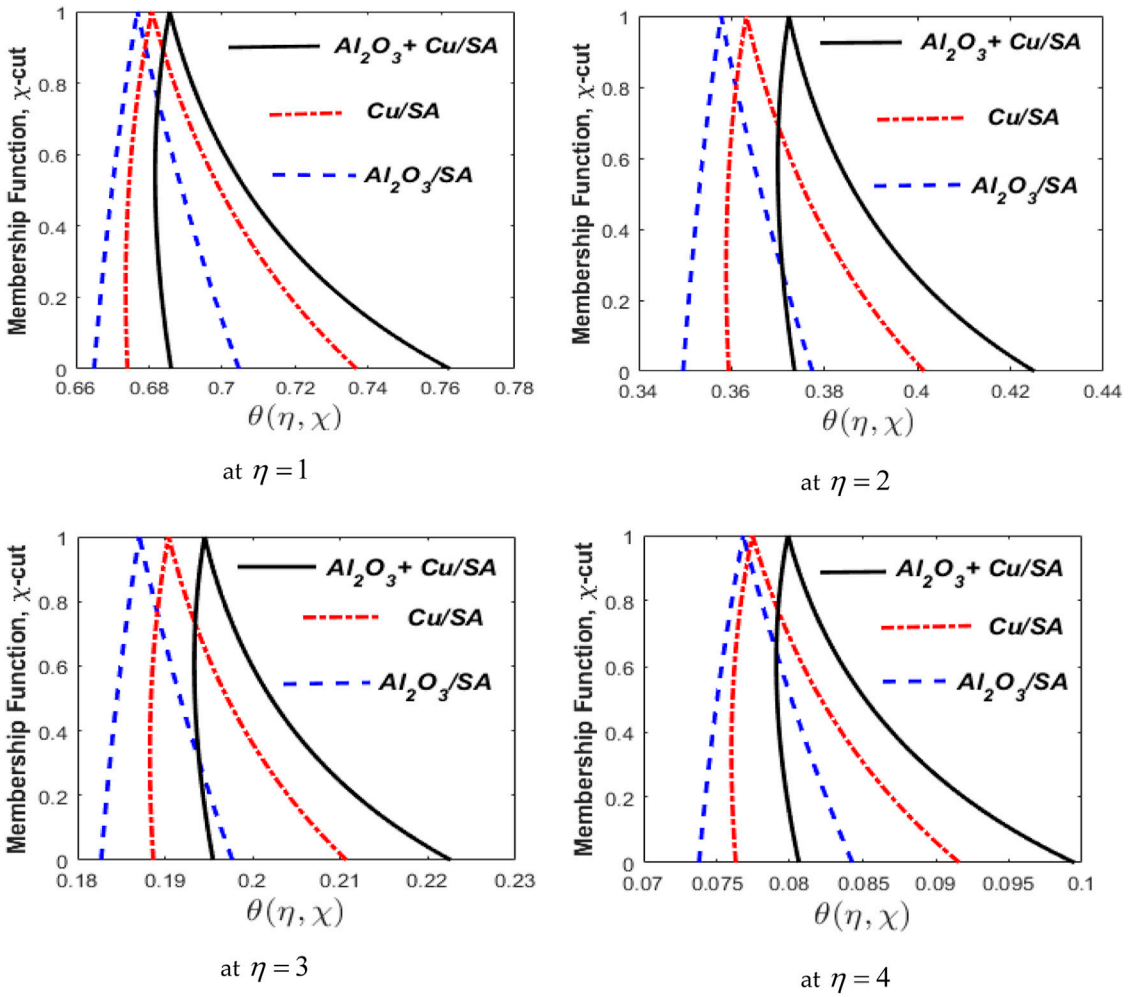

FIGURE 16
Comparison of Al_2O_3/SA, Cu/SA, and Al_2O_3 + Cu/SA hybrid nanofluids for $\omega = 0.5$ and different values of η.

As shown in Figure 12, $f''(0)$ increases with M and decreases as α grows. Due to the Lorentz drag force, an increase in the M value leads to a substantial confrontation to fluid flow, which reduces the fluid velocity and momentum BL thickness, upsurges the velocity, and thus, increases the shear stress of the exponential stretch sheet. The behavior of $f''(0)$, the unsteady parameter (β), and the suction/injection parameter (s) is revealed in Figure 13. It can be detected that the drag force declines with the rise in β and s. Physically, growth in β and s results in an augmentation in the fluid density, due to which more friction is observed by the fluid particles. Figure 14 shows the impact of Nr and H on Nu_x. It is observed that Nu_x reduces with an increase in Nr and H. Nu_x decreases when ϕ_2 increases, while Nu_x increases when ϕ_1 increases, as shown in Figure 15. Physically, heat is emitted from the exponential sheet when enhancing ϕ_1 and ϕ_2.

3.1 Fuzzy results and discussion

Figure 16 portrays the calculated fuzzy temperature using volume fractions of ϕ_1 and ϕ_2 as the TFN [0%, 5%, 10%] for different values of η, 1, 2, 3, and 4; four subplots delineate the fuzzy temperatures for triangular MFs. The vertical axis represents the MF of the fuzzy temperature bend $\chi - \text{cut}\ (0 \le \chi - \text{cut} \le 1)$, and the horizontal axis represents the fuzzy temperature curve with varying values of ?. The resulting fuzzy temperature is TFN, but not symmetric, while a portion of the fuzzy volume is symmetric TFN. These variations might be due to the nonlinearity of the governing FDE. It was also revealed that hybrid nanofluids had a wider width than nanofluids. As a result, the hybrid nanofluid is uncertain according to the TFN. On the other hand, Figure 16 shows the comparison of Al_2O_3/SA (ϕ_1), Cu/SA (ϕ_2), and $Al_2O_3 + Cu/SA$ hybrid nanofluids through MF for numerous values of η. In these figures, we evaluated three scenarios. When ϕ_1 is preserved as TFN and $\phi_2 = 0$, it is signified by blue shapes. When ϕ_2 is preserved as TFN and $\phi_1 = 0$, it is signified by red shapes, and the black lines show that the hybrid nanofluid is non-zero with both ϕ_1 and ϕ_2. It is observed that the temperature change in hybrid nanofluids is more noticeable than in two nanofluids; the performance of hybrid nanofluids is better. To deliver the maximum transmission of heat in hybrid nanofluid joined, the thermal conductivities of Al_2O_3 and Cu. Al_2O_3/SA have a higher heat transfer during the comparison of Al_2O_3/SA and Cu/SA because the thermal conductivity of Al_2O_3 is

TABLE 3 Comparison of current results of $\theta'(0)$ with the work of Haider et al. [36] for variation in *Pr* and *M* when H = 0.0, Nr = 0.0, β = 0.0, and Ec = 0.0

M	Pr	Haider et al. [36] (HAM)	Haider et al. [36] (NM)	Present (HAM)
0	1	0.95478	0.95478	0.95477
	2	1.47146	1.47146	1.47145
	3	1.86907	1.86907	1.86906
	5	2.50012	2.50012	2.50012
	10	3.66027	3.66027	3.66026
1	1	0.56109	0.56109	0.56108

higher than that of *Cu*. The comparative analysis is provided in Table 3 of the proposed technique with prevailing approaches.

4 Conclusion

This study analyzed the unsteady MHD second-grade hybrid (Al_2O_3 + Cu/SA) nanofluid flow caused by the exponentially stretching/shrinking surface. Viscous dissipation, nonlinear thermal radiation, and heat scores/sink are also considered. An analytical approach, the HAM, is implemented for the outcome of the formulated problem. For validity, extant outcomes were equated with prevailing consequences. The impacts of non-dimensional physical parameters on velocity and temperature profiles for second-grade fluid and hybrid nanofluid are examined and discussed via graphs. Furthermore, ϕ_1 and ϕ_2 are said to be TFNs using the χ − cut technique. Comparison and uncertainty are studied through triangular fuzzy graphs. The foremost goals of this study are as follows:

- The fluid velocity is dropped with the magnetic parameter, while the fluid velocity is boosted with the second-grade fluid parameter.
- The fluid temperature increases while the fluid velocity declines with the improvement of ϕ_1 and ϕ_2.
- The fluid temperature boosts against higher values of θ_w, *Nr*, and *H*, whereas the reverse holds for the unsteady parameter, suction parameter, and Prandtl number.
- The fluid velocity grows *versus* the stretching/shirking parameter while the fluid temperature declines.
- The skin friction coefficient is reduced with a rise in unsteady and second-grade parameters while growing with magnetic parameters.
- For higher values of *Nr*, *H*, ϕ_1, and ϕ_2, the surface heat transfer rate decreases.
- The maximum width of the fuzzy fluid temperature of the hybrid nanofluid was observed during a fuzzy analysis using a triangular MF, indicating that the fuzziness level is higher than that of regular nanofluids.
- The Al_2O_3 + Cu/SA hybrid nanofluids showed exceptional capability to increase the heat transfer rate in Al_2O_3/SA and Cu/SA during fuzzy heat transfer analysis compared to regular substances. It has also been observed that the performance of Cu/SA is far better than that of Al_2O_3/SA.

The findings of this study can be used to drive future progress in which the heating system's heat outcome is analyzed with nanofluids or hybrid nanofluids of various kinds (Maxwell, third-grade, Casson, Carreau, micropolar fluids, etc).

Data availability statement

The original contributions presented in the study are included in the article/Supplementary Material; further inquiries can be directed to the corresponding authors.

Author contributions

RZ, MN: conceptualization, methodology, and writing–original draft. MN, MS: data curation, investigation, resources, software, and writing–original draft. IS: formal analysis, supervision, validation, and writing–original draft. IK, AM: funding acquisition, project administration, resources, visualization, and data curation, writing.

Funding

The authors declare financial support was received for the research, authorship, and/or publication of this article. This project was funded by Zhejiang Normal University, Jinhua, Zhejiang, China.

Conflict of interest

The authors declare that the research was conducted in the absence of any commercial or financial relationships that could be construed as a potential conflict of interest.

Publisher's note

References

1. Rajagopal KR. On boundary conditions for fluids of the differential type. In: Sequira A, editor. *Navier- Stokes equations and related nonlinear problems*. New York: Plenum Press (1995). p. 273. doi:10.1007/978-1-4899-1415-6_22

2. Vejravelu K, Roper T. Flow and heat transfer in a second-grade fluid over a stretching sheet. *Int J Non Linear Mech* (1999) 34:1031–6. doi:10.1016/S0020-7462(98)00073-0

3. Rajeswari GK, Rathna SL. Flow of a particular class of non-Newtonian visco-elastic and visco-inelastic fluids near a stagnation point. *Z Angew Math Phys* (1962) 13:43–57. doi:10.1007/BF01600756

4. Garg VK, Rajagopal KR. Flow of a non-Newtonian fluid past a wedge. *Acta Mech* (1991) 88:113–23. doi:10.1007/BF01170596

5. Bilal S, Mustafa Z, Rehman KU, Malik MM. MHD second grade NanoFluid flow induced by a rotatory cone. *J Nanofluids* (2019) 8:876–84. doi:10.1166/jon.2019.1627

6. Mushtaq M, Asghar S, Hossain MA. Mixed convection flow of second grade fluid along a vertical stretching flat surface with variable surface temperature. *Heat Mass Transf* (2007) 43:1049–61. doi:10.1007/s00231-006-0177-8

7. Vieru D, Siddique I, Kamran M. Energetic balance for the flow of a second-grade fluid due to a plate subject to a shear stress. *Comput Maths Appl* (2008) 56(4):1128–37. doi:10.1016/j.camwa.2008.02.013

8. Mahmood A, Fetecau C, Siddique I. Exact solutions for some unsteady flows of generalized second grade fluids in cylindrical domains. *J Prime Res Maths* (2008) 4: 171–80. Available at: https://jprm.sms.edu.pk/media/pdf/jprm/volume_04/jprm10_4.pdf (Accessed 2008).

9. Khan SK, Sanjayanand E. Viscoelastic boundary layer flow and heat transfer over an exponential stretching sheet. *Int J Heat Mass Transf* (2005) 48:1534–42. doi:10.1016/j.ijheatmasstransfer.2004.10.032

10. Rehman A, Farooq G, Ahmed I, Naseer M, Zulfiqar M. Boundary-layer stagnation-point flow of second grade fluid over an exponentially stretching sheet. *Am J Appl Maths Stat* (2015) 3(6):211–9. Available at: http://pubs.sciepub.com/ajams/3/6/1/ (Accessed 2015). doi:10.12691/ajams-3-6-1

11. Nadeem S, Hayat T, Malik MY, Rajput SA. Thermal radiation effects on the flow by an exponentially stretching surface: a series solution. *Z Naturforsch* (2010) 65a: 495–503. doi:10.1515/zna-2010-6-703

12. Ramzan M, Bilal M. Time dependent MHD nano-second grade fluid flow induced by permeable vertical sheet with mixed convection and thermal radiation. *PLoS One* (2015) 10:e0124929. doi:10.1371/journal.pone.0124929

13. Pakdemirli M, Hayat T, Yurusoy M, Abbasbandy S, Asghar S. Perturbation analysis of a modified second-grade fluid over a porous plate. *Nonlinear Anal Real World Appl* (2011) 12:1774–85. doi:10.1016/j.nonrwa.2010.11.010

14. Rehman KU, Shatanawi W, Firdous U. A comparative thermal case study on thermophysical aspects in thermally magnetized flow regime with variable thermal conductivity. *Case Stud Therm Eng* (2022) 44:102839. doi:10.1016/j.csite.2023.102839

15. Nadeem M, Siddique I, Awrejcewicz J, Bilal M. Numerical analysis of a second-grade fuzzy hybrid nanofluid flow and heat transfer over a permeable stretching/shrinking sheet. *Scientific Rep* (2022) 12(1):1631–17. doi:10.1038/s41598-022-05393-7

16. Rehman KU, Shatanawi W, Çolak AB. Levenberg–marquardt training technique analysis of thermally radiative and chemically reactive stagnation point flow of non-Newtonian fluid with temperature dependent thermal conductivity. *Mathematics* (2023) 11(3):753. doi:10.3390/math11030753

17. Rehman KU, Shatanawi W, Laraib K. Mutual impact of thermal radiations and temperature dependent thermal conductivity on non-Newtonian multiple flow regimes. *Case Stud Therm Eng* (2023) 42:102752. doi:10.1016/j.csite.2023.102752

18. Siddique I, Nadeem M, Awrejcewicz J, Pawłowski W. Soret and Dufour effects on unsteady MHD second-grade nanofluid flow across an exponentially stretching surface. *Sci Rep* (2022) 12:11811. doi:10.1038/s41598-022-16173-8

19. Jawad M, Saeed A, Tassaddiq A, Khan A, Gul T, Kumam P, et al. Insight into the dynamics of second grade hybrid radiative nanofluid flow within the boundary layer subject to Lorentz force. *Scientific Rep* (2021) 11:4894. doi:10.1038/s41598-021-84144-6

20. Rehman KU, Shatanawi W, Yaseen S. A comparative numerical study of heat and mass transfer individualities in Casson stagnation point fluid flow past a flat and cylindrical surfaces. *Mathematics* (2023) 11(2):470. doi:10.3390/math11020470

21. Shafiq A, Çolak AB, Sindhu TN. Modeling of Darcy-Forchheimer magnetohydrodynamic Williamson nanofluid flow towards nonlinear radiative stretching surface using artificial neural network. *Int J Numer Methods Fluids* (2023) 95(9):1502–20. doi:10.1002/fld.5216

22. Shafiq A, Çolak AB, Sindhu TN. Significance of EMHD graphene oxide (GO) water ethylene glycol nanofluid flow in a Darcy–Forchheimer medium by machine learning algorithm. *The Eur Phys J Plus* (2023) 138(3):213. doi:10.1140/epjp/s13360-023-03798-5

23. Nadeem M, Siddique I, Ali R, Alshammari N, Jamil RN, Hamadneh N, et al. Study of third-grade fluid under the fuzzy environment with Couette and Poiseuille flows. *Math Probl Eng* (2022) 2022:1–19. doi:10.1155/2022/2458253

24. Smith FT. Steady and unsteady boundary layer separation. *Annu Rev Fluid Mech* (1986) 18:197–220. 18.010186.001213. doi:10.1146/annurev.fl.18.010186.001213

25. White FM. *Viscous fluid flow*. New York: McGraw-Hill (1991). doi:10.3390/math11020470

26. McCroskey WJ. The 1976 freeman scholar lecture: some current research in unsteady fluid dynamics. *J Fluids Eng* (1977) 99:8–39. doi:10.1115/1.3448570

27. Zaib A, Bhattacharyya K, Shafie S. Unsteady boundary layer flow and heat transfer over an exponentially shrinking sheet with suction in a copper-water nanofluid. *J Cent South Univ* (2015) 22:4856–63. doi:10.1007/s11771-015-3037-1

28. Pantokratoras A, Fang T. Sakiadis flow with nonlinear Rosseland thermal radiation. *Phys Scr* (2012) 87(1):015703. doi:10.1088/0031-8949/87/01/015703

29. Dogonchi AS, Ganji DD. Investigation of MHD nanofluid flow and heat transfer in a stretching/shrinking convergent/divergent channel considering thermal radiation. *J Mol Liq* (2016) 224:592–603. doi:10.1016/j.molliq.2016.05.022

30. Khan U, Zaib A, Sheikholeslami M, Wakif A, Baleanu D. Mixed convective radiative flow through a slender revolution bodies containing molybdenum-disulfide graphene oxide along with generalized hybrid nanoparticles in porous media. *Crystals* (2020) 10(9):771. doi:10.3390/cryst10090771

31. Shafiq A, Colak AB, Sindhu TN. Construction of neural network based intelligent computing for treatment of Darcy-forchheimer sisko nanofluid flow with rosseland's radiative process. *Heat Transfer Res* (2023) 54(9):77–98. doi:10.1615/HeatTransRes.2023046617

32. Nadeem M, Siddique I, Bilal M, Anjum K. Numerical study of MHD Prandtl Eyring fuzzy hybrid nanofluid flow over a wedge. *Numer Heat Transfer, A: Appl* (2023) 1–17. doi:10.1080/10407782.2023.2257379

33. Shahzad F, Jamshed W, Eid MR, Safdar R, Putri Mohamed Isa SS, El Din SM, et al. Thermal cooling efficacy of a solar water pump using Oldroyd-B (aluminum alloy-titanium alloy/engine oil) hybrid nanofluid by applying new version for the model of Buongiorno. *Scientific Rep* (2022) 12(1):19817. doi:10.1038/s41598-022-24294-3

34. Nadeem M, Siddique I, Riaz Z, Makhdoum BM, Zulqarnain RM, Sallah M. Numerical study of unsteady tangent hyperbolic fuzzy hybrid nanofluid over an exponentially stretching surface. *Scientific Rep* (2023) 13(1):15551. doi:10.1038/s41598-023-32374-1

35. Bilal M, Tariq H, Urva Y, Siddique I, Shah S, Sajid T, et al. A novel nonlinear diffusion model of magneto-micropolar fluid comprising Joule heating and velocity slip effects. *Waves in random and complex media* (2022). p. 1–17. doi:10.1080/17455030.2022.2079761

36. Haider S, Saeed Butt A, Li YZ, Imran SM, Ahmad B, Tayyaba A. Study of entropy generation with multi-slip effects in MHD unsteady flow of viscous fluid past an exponentially stretching surface. *Symmetry* (2020) 12(3):426. doi:10.3390/sym12030426

37. Lee KJ, Yoon SH, Jang J. Carbon nanofibers: a novel nanofiller for nanofluid applications. *Small* (2007) 3(7):1209–13. doi:10.1002/smll.200700066

38. Shah TR, Ali HM. Applications of hybrid nanofluids in solar energy, practical limitations and challenges: a critical review. *Sol Energ* (2019) 183:173–203. doi:10.1016/j.solener.2019.03.012

39. Huminic G, Huminic A. Hybrid nanofluids for heat transfer applications – a state-of-the-art review. *Int J Heat Mass Transf* (2018) 125:82–103. doi:10.1016/j.ijheatmasstransfer.2018.04.059

40. Choi SU, Eastman J. Enhancing thermal conductivity of fluids with nanoparticles. *ASME Publ Fed* (1995) 231:99–103. doi:10.1002/smll.200700066

41. Ijam A, Saidur R. Nanofluid as a coolant for electronic devices (cooling of electronic devices). *Appl Therm Eng* (2012) 32:76–82. doi:10.1016/j.applthermaleng.2011.08.032

42. Saidur R, Kazi SN, Hossain MS, Rahman MM, Mohammed HA. A review on the performance of nanoparticles suspended with refrigerants and lubricating oils in refrigeration systems. *Renew Sustain Energ Rev.* (2011) 15(1):310–23. doi:10.1016/j.rser.2010.08.018

43. Tiwari RK, Das MK. Heat transfer augmentation in a two-sided lid-driven differentially heated square cavity utilizing nanofluids. *Int J Heat Mass Transf* (2007) 50:2002–18. doi:10.1016/j.ijheatmasstransfer.2006.09.034

44. Suresh S, Venkitaraj KP, Selvakumar P, Chandrasekar M. Effect of Al2O3–Cu/water hybrid nanofluid in heat transfer. *Exp Therm Fluid Sci* (2012) 38:54–60. doi:10.1016/j.expthermflusci.2011.11.007

45. Momin GG. Experimental investigation of mixed convection with water–Al2O3 & hybrid nanofluid in an inclined tube for laminar flow. *Int J Sci Technol Res* (2013) 2: 195–202. doi:10.1002/smll.200700066

46. Waini I, Ishak A, Pop I. Hybrid nanofluid flow towards a stagnation point on an exponentially stretching/shrinking vertical sheet with buoyancy effects. *Int J Numer Methods Heat Fluid Flow* (2020) 31:216–35. doi:10.1108/HFF-02-2020-0086

47. Khan MI. Transportation of hybrid nanoparticles in forced convective Darcy-Forchheimer flow by a rotating disk. *Int Commun Heat Mass Tran* (2021) 122:105177. doi:10.1016/j.icheatmasstransfer.2021.105177

48. Takabi B, Salehi S. Augmentation of the heat transfer performance of a sinusoidal corrugated enclosure by employing hybrid nanofluid. *Adv Mech Eng* (2014) 6:147059. doi:10.1155/2014/147059

49. Aminuddin NA, Nasir NAAM, Jamshed W, Ishak A, Pop I, Eid MR. Impact of thermal radiation on MHD GO-Fe2O4/EG flow and heat transfer over a moving surface. *Symmetry* (2023) 15(3):584. doi:10.3390/sym15030584

50. Sajid T, Pasha AA, Jamshed W, Shahzad F, Eid MR, Ibrahim RW, et al. Radiative and porosity effects of trihybrid Casson nanofluids with Bödewadt flow and inconstant heat source by Yamada-Ota and Xue models. *Alexandria Eng J* (2023) 66:457–73. doi:10.1016/j.aej.2022.11.009

51. Shahzad F, Jamshed W, Eid MR, Ibrahim RW, Aslam F, Isa SSPM, et al. The effect of pressure gradient on MHD flow of a tri-hybrid Newtonian nanofluid in a circular channel. *J Magnetism Magn Mater* (2023) 568:170320. doi:10.1016/j.jmmm.2022.170320

52. Sajid T, Jamshed W, Eid MR, Altamirano GC, Aslam F, Alanzi AM, et al. Magnetized Cross tetra hybrid nanofluid passed a stenosed artery with nonuniform heat source (sink) and thermal radiation: novel tetra hybrid Tiwari and Das nanofluid model. *J Magnetism Magn Mater* (2023) 569:170443. doi:10.1016/j.jmmm.2023.170443

53. Nadeem M, Elmoasry A, Siddique I, Jarad F, Zulqarnain RM, Alebraheem J, et al. Study of triangular fuzzy hybrid nanofluids on the natural convection flow and heat transfer between two vertical plates. *Comput Intelligence Neurosci* (2021) 2021:1–15. doi:10.1155/2021/3678335

54. Zadeh LA. Fuzzy sets. *Inf Control* (1965) 8(3):338–53. doi:10.1016/s0019-9958(65)90241-x

55. Zulqarnain RM, Xin XL, Siddique I, Asghar Khan W, Yousif MA. TOPSIS method based on correlation coefficient under pythagorean fuzzy soft environment and its application towards green supply chain management. *Sustainability* (2021) 13(4):1642. doi:10.3390/su13041642

56. Zulqarnain RM, Siddique I, Ali R, Jarad F, Samad A, Abdeljawad T. Neutrosophic hypersoft matrices with application to solve multiattributive decision-making problems. *Complexity* (2021) 2021:1–17. Article ID 5589874. doi:10.1155/2021/5589874

57. Siddique I, Nadeem M, Khan I, Jamil RN, Shamseldin MA, Akgül A. Analysis of fuzzified boundary value problems for MHD Couette and Poiseuille flow. *Scientific Rep* (2022) 12(1):8368–28. doi:10.1038/s41598-022-12110-x

58. Zulqarnain RM, Saddique I, Jarad F, Ali R, Abdeljawad T. Development of TOPSIS technique under pythagorean fuzzy hypersoft environment based on correlation coefficient and its application towards the selection of antivirus mask in COVID-19 pandemic. *Complexity* (2021) 2021:1–27. Article ID 6634991, 27 pages. doi:10.1155/2021/6634991

59. Siddique I, Zulqarnain RM, Ali R, Jarad F, Iampan A. Multicriteria decision-making approach for aggregation operators of pythagorean fuzzy hypersoft sets. *Comput Intelligence Neurosci* (2021) 2021:1–19. doi:10.1155/2021/2036506

60. Chang SS, Zadeh LA. On fuzzy mapping and control. In: *Fuzzy sets, fuzzy logic, and fuzzy systems: selected papers by lotfi A Zadeh*. World Scientific (1996). p. 180–4. doi:10.1155/2021/2036506

61. Dubois D, Prade H. Towards fuzzy differential calculus Part 3: differentiation. *Fuzzy Sets Syst* (1982) 8(3):613–26. doi:10.1080/00207727808941724

62. Kaleva O. Fuzzy differential equations. *Fuzzy Sets Syst* (1987) 24(3):301–17. doi:10.1016/0165-0114(87)90029-7

63. Nadeem M, Siddique I, Jarad F, Jamil RN. Numerical study of MHD third-grade fluid flow through an inclined channel with ohmic heating under fuzzy environment. *Math Probl Eng* (2021) 2021:1–17. doi:10.1155/2021/9137479

64. Siddique I, Zulqarnain RM, Nadeem M, Jarad F. Numerical simulation of MHD Couette flow of a fuzzy nanofluid through an inclined channel with thermal radiation effect. *Comput Intelligence Neurosci* (2021) 2021:1–16. Article ID 6608684. doi:10.1155/2021/6608684

Nomenclature

Symbols	Description
x, y	Cartesian coordinates
μ_{hnf}	Dynamic viscosity of the hybrid nanofluid
H	Heat source/sink parameter
K	Second-grade fluid parameter
θ_w	Temperature ratio parameter
β	Shrinking/stretching rate parameter
η	Similarity variable
$\theta(\eta)$	Dimensionless temperature
$(\beta_T)_{hnf}$	The thermal expansion coefficient of the hybrid nanofluid
ϕ_1	Volume fraction of alumina nanoparticles
Nu_x	Nusselt number
$\mu_{\tilde{\Omega}}(\eta)$	Membership function
ρ_{hnf}	Density of the hybrid nanofluid
ρ_f	Density of fluid
C_{fx}	Skin friction coefficient
ν_{hnf}	Kinematic viscosity of the hybrid nanofluid
$(\rho C_p)_{hnf}$	Heat capacity of the hybrid nanofluid
δ_f	Electrical conductivity
s	Rate of mass transfer parameter
u, v	Velocity components
μ_f	Dynamic viscosity of the fluid
Pr	Prandtl number
Ec	Eckert number
M	Magnetic parameter
ψ	Stream function
T_w, T_∞	References and ambient temperature
T	Temperature of fluid
$f(\eta)$	Normal component of the flow
ϕ_2	Volume fraction of copper nanoparticles
$\bar{\theta}(\eta, \gamma)$	Fuzzy temperature profile
$f'(\eta, \gamma)$	Fuzzy velocity profile
FDE	Fuzzy differential equation
γ	Level or cut technique
Re_x	Local Reynolds number
ν_f	Kinematic viscosity of fluid
δ_{hnf}	Electrical conductivity of the hybrid nanofluid
Nr	Thermal radiation parameter

Subscripts

S_1	Solid nanoparticles of Cu
S_2	Solid nanoparticles of Al_1O_3